Influence of the power supply on the energy efficiency of an alkaline water electrolyser

Alfredo Ursúa[a], Luis Marroyo[a], Eugenio Gubía[a], Luis M. Gandía[b], Pedro M. Diéguez[c], Pablo Sanchis[a,*]

[a]Department of Electrical and Electronic Engineering, Public University of Navarra Campus de Arrosadía, 31006 Pamplona, Spain

[b]Department of Applied Chemistry, Public University of Navarra, Campus de Arrosadía, 31006 Pamplona, Spain

[c]Department of Mechanical, Energetic and Materials Engineering, Public University of Navarra, Campus de Arrosadía, 31006 Pamplona, Spain

*Corresponding author. Tel.: +34 948169613; fax: +34 948169884.

E-mail address: pablo.sanchis@unavarra.es (Pablo Sanchis).

Abstract

Electric energy consumption represents the greatest part of the cost of the hydrogen produced by water electrolysis. An effort is being carried out to reduce this electric consumption and improve the global efficiency of commercial electrolysers. Whereas relevant progresses are being achieved in cell stack configurations and electrodes performance, there are practically no studies on the effect of the electric power supply topology on the electrolyser energy efficiency. This paper presents an analysis on the energy consumption and efficiency of a 1 $Nm^3 h^{-1}$ commercial alkaline water electrolyser and their dependence on the power supply

topology. The different topologies of power supplies are first summarised, analysed and classified into two groups: thyristor-based (ThPS) and transistor-based power supplies (TrPS). An Electrolyzer Power Supply Emulator (EPSE) is then designed, developed and satisfactorily validated by means of simulation and experimental tests. With the EPSE, the electrolyser is characterised both obtaining its *I-V* curves for different temperatures and measuring the useful hydrogen production. The electrolyser is then supplied by means of two different emulated electric profiles that are characteristic of typical ThPS and TrPS. Results show that the cell stack energy consumption is up to 495 W h Nm^{-3} lower when it is supplied by the TrPS, which means 10 % greater in terms of efficiency.

Keywords: Alkaline water electrolyser; Electrolyser power supply; Hydrogen systems; Energy efficiency.

1. Introduction

The use of hydrogen as a twenty-first century energy carrier can become a reality in accordance with first, the white papers, reports and support policies that national and international public organisms have drawn up and carried out, and second, the research, development and innovation activities that many industrial companies and research centres are developing [1-5].

In this context, the study and analysis of hydrogen generation systems based on water electrolysis is receiving increasing attention particularly when they are supplied by renewable energies. On the one hand, these systems make it possible to obtain an endless fuel for the transport and automobile sector with no generation of greenhouse gasses and other pollutants [6-9]. On the other, water electrolysers have a great potential to contribute to the stabilization,

control and integration of the renewable energies in the electric grids, particularly as the penetration of these energy sources in the electric energy generation system increases [10-16].

Two main types of industrial electrolysis units are being produced today. They basically differ in the type of electrolyte that is used. The first type of electrolysers is characterized by the use of a strongly alkaline aqueous solution of 25-35 wt% potassium hydroxide (KOH) to maximise the ionic conductivity, in which the hydroxide ions (OH^-) are the charge carriers. The reactions that take place in the electrolysis cells of these units are [17]:

Anode: $$2OH^-(aq) \rightarrow \frac{1}{2}O_2(g) + H_2O(l) + 2e^- \quad (1)$$

Cathode: $$2H_2O(l) + 2e^- \rightarrow H_2(g) + 2OH^-(aq) \quad (2)$$

In the second type of electrolysers the electrolyte is an ion conducting membrane that allows H^+ ions to be transported from the anode to the cathode side to recombine forming hydrogen. They are known as proton exchange membrane (PEM) electrolysers [18]. The anodic and cathodic electrochemical reactions taking place here are:

Anode: $$H_2O(l) \rightarrow \frac{1}{2}O_2(g) + 2H^+(aq) + 2e^- \quad (3)$$

Cathode: $$2H^+(aq) + 2e^- \rightarrow H_2(g) \quad (4)$$

Nowadays, the most commonly used electrolysers are the alkaline advanced ones due to their advantageous features. The global energy efficiency of the systems based on these electrolysers can be as high as 73 % referred to the higher heating value (HHV) of hydrogen (3.5 kW h Nm^{-3}), and there are commercial units covering a broad range of hydrogen production rates, from few $Ncm^3\ min^{-1}$ to thousands $Nm^3\ h^{-1}$ [17-19]. Besides, the capital investment cost of PEM electrolysers is, at present, considerably higher in comparison with the alkaline ones mainly because of the use of electrocatalysts based on noble metals (Pt, Ir, Ru), the elevated cost of their membranes (about 200 $ per $Nm^3\ h^{-1}$ of hydrogen at 1 A cm^{-2}),

the requirement of high-quality water and the use of some construction materials such as titanium [20].

The utilization of water electrolysers powered with renewable energy sources is practically nonexistent at industrial scale and there are relatively few demonstration projects. These units have a high cost due to the lack of a developed market for energetic hydrogen. In addition, the cost of the hydrogen produced is highly dependent on the cost of the electrical energy. A report from NREL [19] shows that up to 70 % of the overall costs of the hydrogen produced by an electrolysis plant with a 100 % capacity factor operating along 40 years and powered with commercial electrical energy can be attributed to the cost of the electricity consumed. Hydrogen Technologies (subsidiary of StatoilHydro, Norway), one of the most important companies of water electrolysis equipment, indicates that the electrical energy can be as high as 90 % of the total operating cost of an electrolyser [21]. The contribution of the electric energy price to the hydrogen costs would even increase in case of getting this energy from renewable sources.

Consequently, there is a need for an improvement in global energy efficiency of water electrolysers, and particularly in the reduction of the electric energy consumption of the electrolysis module, without decreasing in so doing the productivity. In this context, several advances have been carried out in alkaline electrolysers in the last years. Concerning the design of the electrolysis stack, new electrolysis cells configurations have been developed to reduce the internal electric resistance. The so-called zero-gap is the configuration adopted by most of the manufacturers. This configuration makes the energy efficiency increase up to 15-30 % [22,23]. A number of investigations have been carried out aiming at achieving further performance improvements. Nagai et al. [24] analyzed the influence of the gas bubbles generated by electrodes separated by different distances in order to investigate the possible existence of an optimum separation that maximises the electrolysis efficiency. Schiller et al.

[25] obtained a reduction in the anodic and cathodic overvoltages of about 15 % when using high performance electrodes produced by means of the vacuum plasma spraying (VPS) technology. They were tested in intermittent operating conditions supplied by a photovoltaic system. It has been reported that additional reductions of energy needs of up to 10 % can be achieved by adding ionic activators into the electrolyte and changing cell geometries [26]. In other works, the process efficiency has been increased with improved membranes properties and materials [27]. There have also been conducted several studies on the influence of the electrolysis pressure on the energy efficiency, although it seems that there is still no general agreement about this question. In this regard, Onda et al. [28] pointed out that high-pressure water electrolysis consumes up to 5 % less energy than atmospheric water electrolysis. On the contrary, Roy et al. [29] found that atmospheric electrolysers have an efficiency that can be up to 16 % higher than that of the high-pressure ones.

In spite of the numerous analyses and efforts that have been performed to reduce the energy consumption of water electrolysers, to the best of our knowledge, there are no specific studies concerning the significance of the electric power supply on the electrolyser efficiency. In addition, it seems that researchers and manufacturers do not share clear and common criteria to select and use the most suitable power supplies.

This work aims to contribute to a better understanding of the influence of the power supplies of alkaline electrolysers in order to stablish selection criteria that optimise their energy efficiency; particularly, the effect of the shape of the electric power supplied to the cell stack on the energy consumption and efficiency of the electrolytic process is considered. This electric power shape depends on the type of power supply, and more precisely on its power electronics converter topology, on the control of the electric variables, mainly current and voltage, and on the harmonic filters at the output of the conversion stage.

Having different types of power supply to feed and test electrolysers is quite difficult and unusual, and most of the times even hardly feasible. In addition, there is a lack of tools that make it possible to analyse the electrolyser efficiency and operation with different power supplies. In order to settle these problems, a novel electric and electronic device is also presented in this paper. The device has been designed and built up by the authors, and has been called Electrolyser Power Supply Emulator (EPSE) [30]. Its main functions are: (a) to characterise and model electrolysers; (b) to emulate the behaviour of wind and photovoltaic generators for supplying electrolysers and analysing their performance with renewable sources [31]; and finally, (c) to emulate different electric supply shapes, including those according to the power supplies currently used both by electrolyser manufacturers and experimental installations, with the objective of evaluating and comparing the influence of the power supply on any commercial alkaline electrolyser. To this end, the EPSE will be used to characterize a commercial alkaline water electrolyser and analyze how its energy consumption and efficiency is influenced by the topology of the electric power supply.

2. Thermodynamics and electrochemical considerations

The processes involved in water electrolysis can be described from thermodynamic and electrochemical bases [17,28,32]. Considering an ideal electrolysis cell operating at constant pressure and temperature, the energy needed for the electrochemical reaction to take place is given by the enthalpy change of the process ΔH.

$$\Delta H = \Delta G + Q = \Delta G + T\Delta S \tag{5}$$

In the last equation ΔG is the change of the Gibbs' free energy, and represents the minimum amount of energy that has to be supplied by means of electricity. In addition,

thermal energy (Q), represented by the term $T\,\Delta S$, where T is the electrolysis temperature and ΔS the change of entropy, is needed.

The reversible cell voltage V_{rev} is the minimum voltage that is required for the water decomposition reaction. Taking into account the Faraday's law, this voltage V_{rev} can be calculated from ΔG as follows:

$$V_{rev} = \frac{\Delta G}{zF} \tag{6}$$

where z is the number of electrons transferred per hydrogen molecule ($z = 2$) and F (96485 C mol^{-1}) is the Faraday constant. If the thermal energy $T\,\Delta S$ is provided by means of electricity, as it is the case in most of the commercial electrolysers, the minimum voltage to carry out water electrolysis with no thermal effect is the thermoneutral cell voltage V_{tn}, which can be expressed as:

$$V_{tn} = \frac{\Delta H}{zF} \tag{7}$$

At standard temperature and pressure (25 ºC and 1 atm) the values of the change of the thermodynamic functions for the water decomposition reaction are as follows: $\Delta G^o = 237$ kJ mol^{-1}, $\Delta S^o = 0.163$ kJ mol^{-1} and $\Delta H^o = 286$ kJ mol^{-1}. According to Eqs. (6) and (7), the resulting reversible and thermoneutral voltages of an electrolytic cell at standard conditions are $V_{rev} = 1.229$ V and $V_{tn} = 1.482$ V, respectively. Whereas temperature, and in a lesser extent pressure, affect the reversible voltage, the thermoneutral voltage remains almost constant due to the fact that the change of the Gibbs' free energy is compensated by the change of the thermal energy term thus remaining the change of enthalpy practically constant. As the electrolysis temperature increases, $T\,\Delta S$ increases whereas ΔG decreases, which means that the proportion of the global energy that has to be supplied by electricity decreases. An increase of pressure has the opposite effect. For example, the reversible voltage decreases to

$V_{rev,\,75\,^{o}C,\,1\,atm} = 1.19$ V when the temperature is 75 ºC, while it increases to $V_{rev,\,25\,^{o}C,\,25\,atm} = 1.299$ V when the pressure increases up to 25 atm.

When a water electrolyser comes into operation, the cell voltage V_{cell} is greater than the reversible cell voltage V_{rev} because of the irreversibilities of the real electrolysis process. In general, the voltage of an electrolytic cell can be expressed by the sum of the contributions of V_{rev} and the overvoltages caused by the irreversibilities:

$$V_{cell} = V_{rev} + V_{ohm} + V_{act} \tag{8}$$

In Eq. (8), V_{ohm} is the overvoltage caused by the so-called ohmic losses. These losses are mainly caused by the straightforward resistance that the electrodes, bipolar plates, current collectors and their corresponding interconnections offer to the flow of electrons, as well as by the resistance to the flow of ions of both the electrolyte and the membrane that separates anode and cathode. This ohmic overvoltage is basically proportional to the electric current flowing through the electrolytic cell. On the other hand, V_{act} is the activation overvoltage, which is related to the electrochemical kinetics. It is caused by the activated nature of the chemical transformations taking place on the surface of the electrodes; as a result, V_{act} is highly dependent on the electrocatalytic properties of the electrode materials. The evolution of the anodic oxygen reaction produces a much higher activation overvoltage than the cathodic evolution of hydrogen. Moreover, the activation overvoltage is strongly non-linear with respect to the electric current.

The relationship between the cell voltage and current (I_{cell}) gives rise to the *I-V* characteristic curve, which is used to characterize the electrochemical behaviour of an electrolytic cell. The *I-V* curve varies considerably with the temperature. For a given current I_{cell}, as the temperature rises, the ohmic and activation losses decrease as well as the reversible voltage V_{rev}, and then V_{cell} decreases. On the contrary, variations in the pressure have a much lower influence on these curves.

Ideally, the hydrogen that is produced by a water electrolysis cell is proportional to the amount of charge (number of electrons) involved by the process. Therefore, the hydrogen production rate is directly proportional to the charge transfer flow, that is, to the electric current (Faraday's law). The hydrogen generated during a particular time interval Δt is the corresponding to the average value (I) of the instantaneous current (i). This is true regardless of the shape of the instantaneous current since the electric charge (q) delivered to the electrolysis process by the power supply depends only on the current average value:

$$I = \frac{1}{\Delta t}\int_0^{\Delta t} i\,dt \quad \Rightarrow \quad q = \int_0^{\Delta t} i\ dt = I\ \Delta t \tag{9}$$

The hydrogen production rate in a bipolar electrolyser, such as the one analysed in this paper, can be expressed as:

$$f_{H2} = \eta_F \frac{n_c\, I_{stack}}{z\, F} \frac{22.41}{1000} 3600 \tag{10}$$

where f_{H2} ($Nm^3\ h^{-1}$) is the hydrogen production rate, η_F is the Faraday efficiency, n_c the number of cells connected in series, and I_{stack} (A) the average value of the electric current flowing through the electrolyser cells stack.

The Faraday efficiency, also known as current efficiency, is defined as the ratio between the electric charge that has been used to produce a particular amount of hydrogen and the total electric charge consumed in the electrolyser cell stack. A Faraday efficiency lower than 1 is caused, on the one hand, by current losses (parasitic currents) in both the cell stack and the different metallic ducts and pipes and, on the other hand, by the hydrogen that is lost through the membranes separating the cathodic and anodic compartments.

The energy consumption per Nm^3 in an electrolyser cell stack in a time interval Δt can be calculated as follows:

$$C_E = \frac{\int_0^{\Delta t} i_{stack}\ v_{stack}\ dt}{\int_0^{\Delta t} f_{H2}\ dt} \tag{11}$$

where C_E (W h Nm^{-3}) is the electrolyser cell stack energy consumption, i_{stack} (A) the instantaneous current flowing through the electrolyser cells stack, and v_{stack} (V) the instantaneous voltage at the electrolyser cell stack terminals.

Finally, the energy efficiency (η_E) of the electrolysis process can be obtained from the ratio between the energy content of 1 Nm^3 of hydrogen generated in terms of its HHV, and the energy consumption C_E:

$$\eta_E(\%) = \frac{HHV\ of\ 1 Nm^3 H_2}{C_E}\ 100 \tag{12}$$

3. Topologies of electrolyser power supplies

The continuous (DC) electric current for the electrolysis process to take place is usually supplied by means of an electrical power supply. Since the electric grids are alternating (AC) sources, the role of the power supply is to condition the AC electric power from the grid and supply the electrolyser stack with a DC current and voltage suitable for the electrolysis process [19]. In addition, the power supply also allows the hydrogen production rate to be controlled by supplying the required electric power to the electrolyser. Although it is not the objective of this paper, it should be noted that there exist more specific applications, such as off-grid systems based on photovoltaic solar energy [33], in which the power conditioning is carried out from a DC level to another DC level since the electric current generated by the photovoltaic modules is continuous. Anyway, these applications have a more scientific and

experimental than commercial interest, and therefore the manufacturers do not usually include this kind of units between their products.

The power supplies for electrolysers can be classified into two main groups depending on the type of semiconductor used. The first one can be called the thyristor-based power supply (ThPS) group, and includes the power supplies based on semiconductors of the thyristor type (e.g. Silicon Controlled Rectifier, SCR), in which only the turn-on control is possible. The second one is the transistor-based power supply (TrPS) group. These power supplies use semiconductors of the transistor type (e.g. IGBT, MOSFET, BJT, etc.), in which both the turn-on and turn-off are controlled [34]. A number of applications of electrolyser power supplies belonging to the ThPS [35-38] and TrPS groups [39-42] have been reported.

Fig. 1 presents two typical electrolyser power supplies of the ThPS group. These supplies are incorporated in the electrolysers produced by Hydrogenics (Canada) [35]. These power units operate connected to the main electric grid. Fig. 1a shows a power supply made up of a step-down power transformer and a three-phase half-controlled rectifier with thyristors and diodes that converts the AC current from the grid into a proper DC current for the desired hydrogen production. On the other hand, Fig. 1b depicts a supply consisting of a three-phase AC/AC thyristor voltage controller, a step-down power transformer connected at the output of the voltage controller, and a diode three-phase rectifier bridge that, from the AC energy delivered at the output of the transformer, generates a DC current whose level can be controlled by means of the thyristor commutations.

Fig. 2 shows two electrolyser power supplies belonging to the TrPS group. Fig. 2a presents a power supply patented by the electrolyser manufacturer AquaGas New Zealand Ltd (presently Environmental Control Products ECP Ltd) to produce hydrogen in a grid-connected system [39]. Fig. 2b introduces a power supply integrated in a hydrogen production system using wind turbine generator [41]. The power unit of Fig. 2a consists as a first step of

a three-phase diode bridge rectifier that provides a three-phase IGBT controlled inverter with an input DC voltage. This inverter generates a high-frequency pseudo-sinusoidal three-phase voltage whose level depends on the desired hydrogen production rate. After that, a high-frequency transformer reduces the amplitude of the pseudo-sinusoidal voltage, and then a diode rectifier bridge and an output filter generate a smooth DC output voltage for the electrolyser. In Fig. 2b a power supply is shown that takes the AC electrical energy from the wind turbine generator and converts it into a DC current by means of a three-phase IGBT controlled rectifier that supplies an electrolytic hydrogen production system.

The power supplies of the ThPS group consist of thyristor converters. These devices are phase-controlled, that is, each thyristor activates once each cycle of the grid frequency (50 Hz or 60 Hz). This low-frequency switching generates low-frequency large-amplitude harmonics in the current and voltage delivered to the electrolysers. This harmonic content could be in theory reduced by incorporating filters at the output of the power supplies. However, filtering low-frequency large-amplitude harmonics involves the use of big filters with a quite high size, weight and cost, making them not suitable for this type of power supplies.

In contrast to the ThPS, the TrPS are based on transistor converters, which are not phase-controlled. These converters operate with high-frequency (even greater than 5 kHz) switching strategies, such as the well-known pulse width modulation, PWM, in which each transistor is turned-on and off hundreds of times each cycle of grid frequency. This generates high-frequency harmonics that make possible the design and implementation of output filters for these converters. As a result, the harmonic content of the DC energy supplied to the electrolyser is very low, that is, the amplitude of the high-frequency harmonics injected into the electrolyser cell stack can be in practice neglected.

4. Electrolyser Power Supply Emulator

4.1. Description of the electronic equipment

The schematic description of the EPSE is shown in Fig. 3. It has a nominal power of 10.5 kW, and can emulate instantaneous currents and voltages up to 300 A and 70 V and permanent currents and voltages of 150 A and 70 V. The EPSE basically consists of a power stage, a control stage, a measurement stage and a microcontroller. The power stage includes a transformer, an electronic converter and an output filter. The control stage implements a feedback control loop of the current supplied to the electrolyser (i_{stack}) by means of generating the corresponding control signal D for the electronic converter from a proportional-integral controller. The measuring stage measures the variables of both the electronic converter and the electrolyser, and then sends these measurements to both the current control loop and the microcontroller after filtering them. The microcontroller, which consists of a digital signal processor (DSP) from dSPACE [43] placed on a personal computer, has as main task the generation of the desired profile of the electric supply to the electrolyser cell stack. This profile is given to the electrolyser in terms of the corresponding reference current waveform for the current control loop ($i_{stack,ref}$). In addition, the microcontroller carries out the data adquisition, monitoring, processing and storage, as well as the programming of the equipment protections as a function of the measured variables.

Fig. 4 shows a detailed scheme of the power stage of the EPSE. The three-phase diode bridge rectifies the transformed AC voltages (r, s, t) and the capacitor C_{DC} provides a stabilised DC input voltage (v_{DC}) for the DC/DC converter. This is a buck converter based on IGBT that supplies the electrolyser with the desired current i_{stack}. Its switching frequency is 20 kHz. The current loop implemented in the control stage generates, according to the reference $i_{stack,ref}$, the switching signals for the converter to control the current i_L that flows through the output inductance L_m. This loop has a 5.6 kHz bandwidth, which means a very

fast dynamics that allows the current i_{stack} to track with high accuracy the reference $i_{stack,ref}$. Finally, the output filter consists of two capacitors C_{f1} and C_{f2}, an inductance L_f, and a damping and dissipation resistor R_f [44]. Together with the inductance L_m, the filter reduces and practically cancels the high-frequency switching harmonics, damps possible resonant modes that can appear between the different elements of the circuit, and minimises the losses in the resistor.

4.2. Simulation and experimental validation

Before physically implementing the EPSE, it was first simulated with the help of Matlab/Simulink software. The simulation model incorporated the power, measuring and control stages, including filters, delays, thermal losses in the elements and switching of the semiconductors. Therefore, the model represents a close approximation to the real system. A variety of scenarios were simulated, such as step response, current ramps, load changes, tracking of sinusoidal currents, etc. Once the capability of the EPSE to reproduce the desired electric power profiles was satisfactorily checked by the simulation results, the physical implementation of the EPSE was designed, developed and carried out.

In order to experimentally validate the built equipment, it was subjected to the same tests that were previously simulated. Two representative simulation and experimental results ilustrating the features, performance and capabilities of the equipment are shown in Figs. 5 and 6. In these figures, the control loop reference current $i_{stack,ref}$ (named "reference current" in the graphs), the DC/DC converter current i_L ("converter current"), and the EPSE output current i_{stack} ("output current") and output voltage v_{stack} ("output voltage") are shown. Although in this case the load is not a water electrolyser but the previously described resistors, the nomenclature used for currents and voltages, and particularly for the subscripts of i_{stack} and v_{stack} is maintained along the paper.

Fig. 5 shows the simulation, on the left-hand side, and the experimental behaviour, on the right-hand side, of the EPSE when faced with a step in the current reference $i_{stack,ref}$ from 10 to 120 A using a resistive load of 0.36 Ω. It is remarkable the good performance of the output filter since the 20 kHz switching ripple is 9 % in the converter current i_L and 1 % in the output current i_{stack}. As concerns i_{stack}, the rising times in the simulation and in the experimental test are 365 µs and 380 µs, respectively, while the settling times are in both cases 1.8 ms. Regarding the overshoot, it achieves 22 % in the simulation and 16 % in the experimental test. Obviously, the voltage v_{stack} behaves with the same tendency as the current i_{stack} since a resistive load is used.

Fig. 6 shows a test in which the current reference $i_{stack,ref}$ is a sinusoidal waveform with an amplitude of 20 A and a frequency of 900 Hz, superimposed to a DC continuous value of 80 A. The resistive load is now 0.42 Ω. The simulation and experimental results show how both currents, i_L and i_{stack}, are able to track the reference $i_{stack,ref}$ with high accuracy and no delay, despite the important amplitude (20 A) and high speed (900 Hz) of the sinusoidal component of the reference. Again, the voltage v_{stack} is obviously proportional to the current i_{stack} due to the resistive load.

It can be concluded that there is a very good agreement between the experimental behaviour of the constructed equipment and the simulation model. Moreover, the correct operation of the EPSE and its capability to emulate electric profiles of power supplies based both on thyristors (ThPS, with high content in low frequency harmonics) and transistors (TrPS, with low or even null harmonic content) have been satisfactorily validated.

It can be concluded that there is a very good agreement between the experimental behaviour of the constructed equipment and the simulation model. Moreover, Figs. 5 and 6 highlight the accuracy and fast dynamics (bandwidth of 5.6 kHz) of the EPSE current control loop when tracking quick reference currents (900 Hz in the test shown in Fig. 6). As a

consequence, the unit will be able to emulate the electric profile of power supplies based both on thyristors (ThPS, which include significant low-frequency harmonics up to eighteenth-order, 900 Hz) and transistors (TrPS, with negligible harmonic content).

5. Experimental setup

The experimental study developed in this work has been carried out at the Hydrogen Laboratory of the Public University of Navarra. This laboratory is equipped with a commercial water electrolyser H2 IGen 300/1/25 manufactured by Vandenborre (currently, Hydrogenics) [35]. The electrolyser, which is shown in Fig. 7, is of the so-called *advanced alkaline electrolyser* type. It can operate at absolute pressures between 5 and 26 bar, and temperatures between 2 and 65 ºC. The cell stack is composed of 22 circular electrolysis cells of 300 cm^2 each, connected in series according to a bipolar stack design. Each electrolysis cell contains a pair of electrodes (anode and cathode) separated by an inorganic ion-exchange membrane and jointly assembled and compressed to obtain a *zero gap configuration*. This means that the distance between the different elements of the cell stack is extremely low with the aim of achieving a highly efficient process. The electrolyte is a 30 wt% KOH aqueous solution to get the required high conductivity. The water used for the electrolysis process is deionised by means of an ion-exchange resin bed to obtain a permanent conductivity lower than 5 μS cm^{-1}. Owing to the design of this electrolyser model, there is no need for pumps for either the electrolyte circulation or the water filling mechanisms. The nominal production rate is 1 Nm^3 h^{-1} at an average DC current of 120 A; the production range is between 33 and 100 % of this value. According to the manufacturer specifications, the overall energy consumption of the electrolyser, including peripherals, valves, instrumentation, etc., is 4.9 kWh Nm^{-3}, out of which the cell stack accounts for 4.3 kWh Nm^{-3}.

The laboratory also includes the EPSE, described in section 4. The instrumentation consists of a digital oscilloscope, two current probes and a differential voltage probe. A precision power analyzer Yokogawa WT3000 and a digital sensor mass flow meter Bronkhorst/IN-FLOW were also used for measuring the electrical power and energy consumption by the cell stack and assessing the hydrogen production rate of the electrolyser, respectively.

6. Results and discussion

6.1. Alkaline water electrolyser characterization

The EPSE was used to characterize the performance of the electrolyser since commercial units lack power supplies harbouring the necessary potential for evaluating the electrochemical behaviour of the electrolyser cell stack. Commercial alkaline electrolysers have a lower operating limit, generally between 25 – 40 % of the nominal current, mainly to prevent the formation of potentially flammable mixtures of hydrogen and oxygen by gas diffusion through membranes at low electric currents. This limitation does not allow commercial power supplies to be used for obtaining cell stack *I-V* curves throughout the complete current range. Furthermore, to establish *I-V* curves correctly, the power supply must not introduce any harmonic in the electrolyser cell stack. Due to the great non linearity of the *I-V* curves, the presence of harmonics in current and voltage, as it happens in most of the commercial units, distorts these curves when average current and voltage values are considered. In addition, the existence of harmonics of the same order in the voltage and current generates an additional power supplied to the cell stack that is not reflected in the *I-V* curves. This additional power depends on the root-mean-square values of the harmonics and on the phase lags between current and voltage same order harmonics. Therefore, power

supplies that introduce harmonics in the electrolyser cell stack should not be used to determine *I-V* curves since the information obtained is incorrect.

In this study, *I-V* curves were established through programming the EPSE leading to an automatic process. The objective of this assay was to obtain *I-V* curves from 120 A (electrolyser nominal current) to 0 A, for a temperature range from room to nominal value (65 ºC). With the aim of carrying out this experiment in a correct way, a compromise arises between: *i*) the necessities of capturing each *I-V* curve as fast as possible in order to get data at virtually constant temperature and minimize the time the electrolyzer operates below the lowest current limit, and *ii*) the need of obtaining each curve sufficiently slowly so as to achieve that the electrolyser works in a permanent regime, in which the cell stack voltage is stable for each current value. To this end, the dynamics of the electrolyser was investigated. Results showed that the electrolyser can be considered as working at permanent regime when the lineal current variation from 120 to 0 A is carried out in at least 10 s. Likewise, the temperature can be considered constant when changes in current from 120 to 0 A are performed in less than 40 s, since its fluctuation was then lower than ± 0.2 ºC.

The protocol of the programmed test in the EPSE was as follows: (1) The electrolyser was supplied with a DC current of 120 A for 150 s; (2) a descending current slope from 120 to 40 A for 10 s was then introduced; (3) finally, another current slope from 40 to 0 A for 20 s was set up. This process was continuously repeated until the electrolyser temperature reached the maximum allowable value of 65 ºC. Step 3 takes twice the time of step 2 to be able to capture non linearity of *I-V* curves at low current ranges in the most precise manner.

In the EPSE database, 1500 current points and their corresponding voltage values, as well as one temperature data, were recorded for each *I-V* curve. Pressure was considered reasonably stable, showing fluctuations lower than ± 0.4 bar along the assay. Several *I-V* curves at different temperatures were obtained according to this procedure. The temperature

changed slowly due to the energy dissipated as heat in the cells stack. Since a *I-V* curve was captured every 3 min, the temperature variation for each curve was negligible, giving rise to a great precision and reliability of the experimental results.

Fig. 8 shows the experimental characterization of the electrochemical behaviour of the electrolyser cell stack at an absolute operating pressure of 20 bar. Figs. 8a and 8b illustrate the evolution of *I-V* curves and power - current curves (*I-P* characteristic curves), respectively, in the temperature range from 15 to 65 ºC. As shown in Fig. 8a, a linear behaviour in the current interval from 120 to about 50 A can be noticed. This is mainly a consequence of the linear behaviour of the ohmic overvoltage and also of the relatively constant activation overvoltage under high currents. Below 50 A a non linear tendency is manifested due to the predominance of the activation overvoltage with respect to ohmic overvoltage at low currents. It can be also clearly seen how for a given current the voltage decreases at increasing temperatures. Fig. 8b shows the *I-P* curves obtained from the experimental *I-V* curves plotted in Fig. 8a. The power tends to decrease as the temperature increases; this is more evident at low temperatures. Such tendency, especially in the case of high currents (120-50 A), is linked to the strong dependence of the electrolyte conductivity (σ) on temperature [45]. It is also remarkable that at a nominal current of 120 A, the cell stack consumes up to 5.6 % more electrical power when it operates at 15 ºC (4765 W) than when operating at 65º C (4495 W).

The EPSE was also used to obtain the electrolyser hydrogen production rate. Fig. 9 shows the hydrogen production of the alkaline electrolyser in the current range from 40 to 120 A and operating conditions of 20 bar and 65 ºC. The useful hydrogen production, that is, the one determined with the mass flow meter, is shown as "H_2 measured". Each hydrogen production point was measured for 5 h under steady-state conditions and data were taken with a sampling frequency of 5 s. In this figure, the "ideal" (100 % Faraday efficiency) hydrogen production is included. To calculate the ideal production, Eq. (10) with $\eta_F = 1$ was used. Fig. 9 also shows

the hydrogen losses calculated as the difference between the ideal and the measured production. Some of these losses are due to the Faraday or current efficiency ($\eta_F < 1$). The rest of the losses are mainly caused by the hydrogen that is used in both the sensor analyzing the purity of the hydrogen produced (oxygen content of the hydrogen) and the mechanism feeding water to the electrolyser, and then sent to the vent lines. The feeding water mechanism uses hydrogen to pressurise water in order that it can be fed by gravity; however, this hydrogen is subsequently safely vented.

Analysing the hydrogen losses shown in Fig. 9, it can be noted that they range from 19.2 % (at 40 A) to 16.5 % (at 120 A) of the "ideal" hydrogen production. This is obviously a significant proportion. The nominal hydrogen production, that is, the production taking place when a DC current of an average value of 120 A flows through the cell stack, is 0.918 $Nm^3 h^{-1}$, which is 8.2 % lower than the nominal production indicated in the electrolyser specifications (1 $Nm^3 h^{-1}$).

6.2. Effect of the power supply topology on the electrolyser energy consumption and efficiency

In order to evaluate the energy efficiency of the electrolytic process as a function of the type of power supply, two conversion topologies representative of the ThPS and TrPS groups were selected. The first power supply, which belongs to the ThPS group, is the one that was shown in Fig. 1a. The second power supply is the one presented in Fig. 2a and belongs to the TrPS group. By means of the EPSE and the experimental setup described in the preceding section, both power supplies were emulated to supply the electrolyser. The results obtained are shown in Figs. 10 and 11.

Fig. 10 shows the results of the emulation of the electric shape (current and voltage) characteristic of the ThPS power supply of Fig. 1a assuming a 50 Hz AC electric grid. The

electrolyser was fed to obtain the nominal hydrogen production rate (1 $Nm^3\ h^{-1}$ at an average DC current of 120 A). As shown in Fig. 10a, the cell stack current is a pulse waveform with peak values of about 280 A and valley values of 0 A. Concerning the voltage, oscillations in its waveform are similar to the ones of the current. In addition, both waveforms are in phase. This demonstrates the strongly resistive behaviour of the electrolyser and makes the power supply operate in the discontinuous conduction mode. The frequency of both periodic waveforms is 150 Hz, with average values of 120 A for current and 38 V for voltage. The harmonic distribution of the current is shown in Fig. 10b. As expected for this type of power supplies, it is greatly influenced by the low-frequency harmonics, such as third-order (amplitude of 155 A at 150 Hz), sixth-order (18 A at 300 Hz) and ninth-order harmonics (22 A at 450 Hz).

The harmonic content of a DC current waveform can be quantified by means of the so-called Form Factor (FF), given by [34]:

$$\mathrm{FF} = \frac{\sqrt{\sum_{n=1}^{n=N}\left(\frac{i_n}{\sqrt{2}}\right)^2 + (I_{DC})^2}}{I_{DC}} \tag{13}$$

where i_n (A) is the amplitude of the n-order harmonic of the current, N is the maximum harmonic order which is considered and I_{DC} (A) is the DC component of the current, that is, its average value. A high FF value means that the harmonics have an important weight in comparison with the DC component. For the current waveform of Fig. 10a, the value of the Form Factor is FF = 1.36. This is quite a high value and reveals a high harmonic content.

Fig. 11 shows the results of supplying the electrolyser cell stack with the current and voltage profiles generated by the TrPS power supply shown in Fig. 2a. The supply is also assumed to be connected to a 50 Hz electric AC grid and the electrolyser is operated at nominal hydrogen production rate. Fig. 11a shows that the power supply generates a current

and voltage for the cell stack of 120 A and 37 V, respectively. In contrast to the previous ThPS power supply, the values of the current and voltage are both average and instantaneous values, since there are no appreciable oscillations, that is, harmonics, in the waveforms. The harmonic content of the current is shown in Fig. 11b, and corroborates the low harmonic distortion, hardly appreciable. This negligible presence of harmonics in current, and consequently in voltage, is due to the high-frequency filtering stage at the output of the power supply. For this case, the FF calculated by means of Eq. (13) gives a value of FF = 1, which means that the current is in practice exempted from harmonics.

Once the shapes of both ThPS and TrPS supplies were characterised, different tests were carried out to compare the behaviour of the electrolyser under these power supplies. In order to make the comparison of the results possible, it is necessary that, according to Eq. (9), the average value of the currents delivered by both emulated power supplies is the same. In so doing, the hydrogen production rate will also be the same. The tests were carried out for DC average currents ranging from 40 to 120 A. The electrolyser operating pressure and temperature were set at 20 bar and 65 ºC, respectively.

The upper graph of Fig. 12 shows the electric power consumption of the electrolyser cell stack when fed with the TrPS and the ThPS power supplies. The power consumption was measured with the precision power analyser. The consumption in case of having an "ideal" electrolysis process with no losses is also shown. This ideal power consumption has been calculated as the product of the thermoneutral voltage, the cell stack current and the number of cells connected in series ($n_c\ V_{tn}\ I_{stack}$). The power losses (Joule losses) caused by the process irreversibilities were obtained as the difference between the ideal power consumption and the consumption with the ThPS and the TrPS power supplies and are shown in the lower graph of Fig. 12. As can be seen, the losses vary from 195 W at 40 A to 1055 W at 120 A when the electrolyser is supplied by the ThPS, while they are much lower in the case of TrPS,

varying from 65 W at 40 A to 600 W at 120 A. In fact, the losses in the stack power consumption are between 1.75 (at 120 A) and 3 (at 40 A) fold higher when using the ThPS. That means that the relative difference of the losses between both power supplies is considerably higher at low currents. The reason is that as the current supplied by the ThPS gets lower, the harmonic distortion increases. At 120 A, FF is 1.36 according to Eq. (13), while it increases up to 1.86 at 40 A. In contrast, FF is always 1 for the current supplied by the TrPS regardless of the current amplitude.

Fig. 13 shows the comparison of the experimental energy consumption (C_E, upper graph) and efficiency (η_E, lower graph) when the electrolyser operates with the TrPS and ThPS. The energy consumption was obtained by means of Eq. (11), where the power consumed by the electrolyser cell stack ($i_{stack}\, v_{stack}$) was measured with the precision power analyzer and the hydrogen production rate (f_{H2}) with the digital mass flow meter. The energy efficiency was calculated by means of Eq. (12).

These results show that the lowest energy consumption, and consequently the highest efficiency, appears with both power supplies at a current of about 48 A. At this point, the electrolyser consumes 4995 W h Nm^{-3} with the ThPS and 4560 W h Nm^{-3} with the TrPS, while the efficiencies are 70.9 % and 77.6 %, respectively. On the other hand, the highest energy consumption, that is the lowest efficiency, takes place with both power supplies when the electrolyser operates at nominal production (120 A). The consumptions, in this case, are 5390 W h Nm^{-3} with the ThPS and 4895 W h Nm^{-3} with the TrPS, being the efficiencies 65.7 % and 72.3 %, respectively. These consumptions are significantly higher than the one indicated in the electrolyser especifications, namely 4300 W h Nm^{-3}, under similar operating conditions. Compared with this value, the consumption is 1090 W h Nm^{-3} higher with the ThPS and 595 W h Nm^{-3} with the TrPS. Anyway, on comparing both power supplies, the consumption is up to 495 W h Nm^{-3} greater when using the ThPS instead of the TrPS, being

the efficiency between 9.2 and 10 % greater with the TrPS. The experimental results highlight the great importance of the electric power supply topology in the efficiency of the electrolyser cell stack.

As a final remark, it is important to emphasize that this study has been focused on the analysis of the energy consumption and efficiency from the point of view of the electrolysis process. In this respect, a power supply of the TrPS type is clearly the most suitable. However, it is also important to analyse the energy efficiency of the power supplies themselves in order to optimize the efficiency of the complete hydrogen system. The authors are now working on this issue.

7. Summary and conclusions

In this paper, an Electrolyser Power Supply Emulator (EPSE) has been designed, developed and built. The EPSE makes it possible to characterise commercial alkaline water electrolysers and analyse their energy consumption as a function of the electric power supply. The validation of the EPSE has been accomplished with a very good accordance between the experimental behaviour of the device and its simulation model. Due to the design features and quick dynamics of its current control loop (bandwidth of 5.6 kHz), the EPSE has a high accuracy in the tracking of the references. As a result, the EPSE is capable of emulating the electric profile of the different power supplies that are commonly used with commercial water electrolysers.

A commercial electrolyser has been characterised. Its characteristic *I-V* curves covering the whole current range from 0 A to its nominal value (120 A), and for a temperature range from room value (15 ºC) up to the nominal limit (65 ºC) have been determined. Besides, the hydrogen production has been measured for currents ranging between 40 to 120 A.

Two representative power supplies (a thyristor-based power supply, ThPS, and a transistor-based power supply, TrPS) have been emulated to feed the water electrolyser. The electrolyser energy consumption and efficiency have been measured for both supplies. The lowest energy consumption and the corresponding highest electrolyser efficiency are 4995 W h Nm^{-3} and 70.9 %, respectively, with the ThPS; while they are 4560 W h Nm^{-3} and 77.6 %, respectively, with the TrPS. The energy efficiency of the electrolyser cell stack is between 9.2 and 10 % higher when using the TrPS in comparison with the ThPS.

Acknowledgements

We gratefully acknowledge Acciona Biocombustibles and Ingeteam, and particularly Mr. Eugenio Guelbenzu and Mr. Javier Pérez, for their financial and permanent support. We also acknowledge the Spanish Ministry of Science and Technology (grant number DPI2006-15703-C02-02) and the Department of Education of the Government of Navarra for their financial support.

References

[1] Conte M, Iacobazzi A, Ronchetti M, Vellone R. Hydrogen economy for a sustainable development: state-of-the-art and technological perspectives. J Power Sources 2001; 100: 171-187.

[2] Dunn S. Hydrogen futures: toward a sustainable energy system. Int J Hydrogen Energy 2002; 27: 235-264.

[3] Elam CC, Padró CEG, Sandrock G, Luzzi A, Lindblad P, Hagen EF. Realizing the hydrogen future: the International Energy Agency's efforts to advance hydrogen energy technologies. Int J Hydrogen Energy 2003; 28: 601-607.

[4] Barreto L, Makihira A, Riahi K. The hydrogen economy in the 21st Century: a sustainable development scenario. Int J Hydrogen Energy 2003; 28: 267-284.

[5] Barbir F, Plass HJ, Veziroglu TN. Modeling of hydrogen penetration in the energy market. Int J Hydrogen Energy 1993; 18: 187-195.

[6] Plass HJ, Barbir F, Miller HP, Veziroglu TN. Economics of hydrogen as a fuel for surface transportation. Int J Hydrogen Energy 1990; 15: 663-668.

[7] Nadal M, Barbir F. Development of a hybrid fuel cell/battery powered electric vehicle. Int J Hydrogen Energy 1996; 21: 497-505.

[8] Granovskii M, Dincer I, Rosen MA. Life cycle assessment of hydrogen fuel cell and gasoline vehicles. Int J Hydrogen Energy 2006; 31: 337-352.

[9] Granovskii M, Dincer I, Rosen MA. Exergetic life cycle assessment of hydrogen production from renewables. J Power Sources 2007; 167: 461-471.

[10] Sherif SA, Barbir F, Veziroglu TN. Wind energy and the hydrogen economy-review of the technology. Solar Energy 2005; 78: 647-660.

[11] Troncoso E, Newborough M. Implementation and control of electrolysers to achieve high penetrations of renewable power. Int J Hydrogen Energy 2007; 32: 2253-2268.

[12] Segura I, Pérez-Navarro A, Sánchez C, Ibáñez F, Payá J, Bernal E. Technical requirements for economical viability of electricity generation in stabilized wind parks. Int J Hydrogen Energy 2007; 32: 3811-3819.

[13] Shaw S, Peteves E. Exploiting synergies in European wind and hydrogen sectors: a cost-benefit assessment. Int J Hydrogen Energy 2008; 33: 3249-3263.

[14] Mantz RJ, De Battista H. Hydrogen production from idle generation capacity of wind turbines. Int J Hydrogen Energy 2008; 33: 4291-4300.

[15] Jørgensen C, Ropenus S. Production price of hydrogen from grid connected electrolysis in a power market with high wind penetration. Int J Hydrogen Energy 2008; 33: 5335-5344.

[16] Bernal-Agustín JL, Dufo-López R. Hourly energy management for grid-connected wind-hydrogen systems. Int J Hydrogen Energy 2008; 33: 6401-6413.

[17] Ulleberg Ø. Modeling of advanced alkaline electrolyzers: a system simulation approach. Int J Hydrogen Energy 2003; 28: 21-23.

[18] Barbir F. PEM electrolysis for production of hydrogen from renewable energy sources. Solar Energy 2005; 78: 661-669.

[19] Ivy J. Summery of electrolytic hydrogen production: milestone completion report, NREL/MP-560-36734., September 2004.

[20] Grigoriev SA, Porembsky VI, Fateev VN. Pure hydrogen production by PEM electrolysis for hydrogen energy. Int J Hydrogen Energy 2006; 31: 171-175.

[21] http://www.electrolysers.com (accessed July 2008).

[22] Wendt H, Imarisio G. Nine years of research and development on advanced water electrolysis. A review of the research programme of the Commission of the European Communities. J Appl Electrochem 1988; 18: 1-14.

[23] Hug W, Divesek J, Mergel J, Seeger W, Steeb H. Highly efficient advanced alkaline electrolyzer for solar operation. Int J Hydrogen Energy 1992; 17: 699-705.

[24] Nagai N, Takeuchi M, Kimura T, Oka T. Existence of optimum space between electrodes on hydrogen production by water electrolysis. Int J Hydrogen Energy 2003; 28: 35-41.

[25] Schiller G, Henne R, Mohr P, Peinecke V. High performance electrodes for an advanced intermittently operated 10-kW alkaline water electrolyzer. Int J Hydrogen Energy 1998; 3: 761-765.

[26] Kaninski MPM, Maksic AD, Stojic DL, Miljanic SS. Ionic activators in the electrolytic production of hydrogen-cost reduction-analysis of the cathode. J Power Sources 2004; 131: 107-111.

[27] Vermeiren P, Adriansens W, Moreels JP, Leysen R. Evaluation of the Zirfon separator for use in alkaline water electrolysis and Ni-H_2 batteries. Int J Hydrogen Energy 1998; 23: 321-324.

[28] Onda K, Kyakuno T, Hattori K, Ito K. Prediction of production power for high-pressure hydrogen by high-pressure water electrolysis. J Power Sources 2004; 132: 64-70.

[29] Roy A, Watson S, Infield D. Comparison of electrical energy efficiency of atmospheric and high-pressure electrolysers. Int J Hydrogen Energy 2006; 31: 1964-1979.

[30] Guelbenzu E, Sanchis P, Ursúa A, Marroyo L, Gandía LM, Diéguez PM. Electrical-electronic device for measuring and emulating wind power systems. International Patent Application Nr. WO2007/057493.

[31] Gandía LM, Oroz R, Ursúa A, Sanchis P, Diéguez PM. Renewable Hydrogen Production: Performance of an Alkaline Water Electrolyzer Working under Emulated Wind Conditions. Energy & Fuels 2007; 21: 1699-1706.

[32] LeRoy RL, Bowen CT, LeRoy DJ. The Thermodynamics of Aqueous Water Electrolysis. J Electrochem Soc 1980; 127: 1954-1962.

[33] Kélouwani S, Agbossou K, Chahine R. Model for energy conversion in renewable energy system with hydrogen storage. J Power Sources 2005; 140: 392-399.

[34] Mohan N, Undeland TM, Robbins WP. Power Electronics: Converters, Applications, and Design. 3th ed. USA: John Wiley & Sons; 2003. p. 38-42.

[35] http://www.hydrogenics.com (accessed July 2008).

[36] http://www.accagen.com (accessed July 2008).

[37] Dutton AG, Bleijs JAM, Dienhart H, Falchetta M, Hug W, Prischich D, Ruddell AJ. Experience in the design, sizing, economics, and implementation of autonomous wind-powered hydrogen production systems. Int J Hydrogen Energy 2000; 25: 705-722.

[38] Kim JH. Power pack for hydrogen and oxygen gas generator. Korean Patent Application Nr. KR20030043817.

[39] Green AW. An AC-DC Power Supply. International Patent Application Nr. WO97/17753.

[40] De Battista H, Mantz RJ, Garelli F. Power conditioning for a wind-hydrogen energy system. J Power Sources 2006; 155: 478-486.

[41] Oohara S, Ichinose M, Futami M, Matsutake M, Fujii K, Ide K, Itabashi T, Tamura J. Hydrogen production system using wind turbine generator. United States Patent Application Nr. 11/654684.

[42] Cavallaro C, Chimento F, Musumeci S, Sapuppo C, Santonocito C. Electrolyser in H2 Self-Producing Systems Connected to DC Link with Dedicated Phase Shift Converter. International Conference on Clean Electrical Power 2007; 632-638.

[43] dSPACE. http://www.dspace.com (accessed July 2008).

[44] Sanchis P, López J, Ursúa A, Gubía E, Marroyo L. On the Testing, Characterization, and Evaluation of PV Inverters and Dynamic MPPT Performance Under Real Varying Operating Conditions. Prog Photovolt Res Appl 2007; 15: 541-556.

[45] Gilliam RJ, Graydon JW, Kirk DW, Thorpe SJ. A review of specific conductivities of potassium hydroxide solutions for various concentrations and temperatures. Int J Hydrogen Energy 2007; 32: 359-364.

Figures

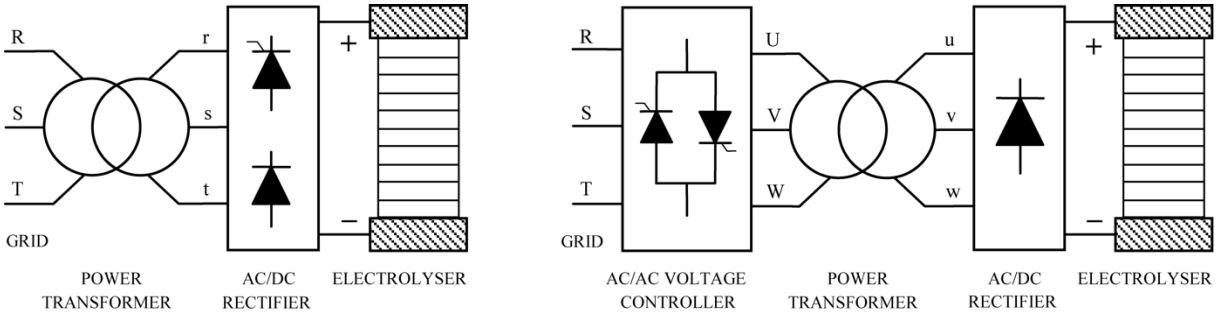

Fig. 1. Thyristor-based power supplies (ThPS). (a) Three-phase half controlled rectifier with thyristors and diodes. (b) Three-phase thyristor voltage controller and diode full-bridge rectifier.

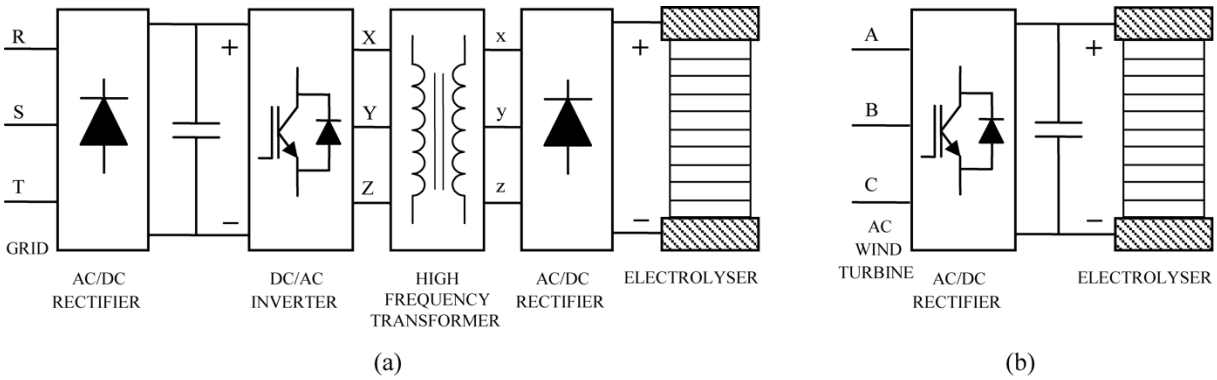

Fig. 2. Transistor-based power supplies (TrPS). (a) Three-phase diode full-bridge rectifier, IGBT inverter, high frequency transformer and diode full-bridge rectifier. (b) Three-phase IGBT controlled rectifier.

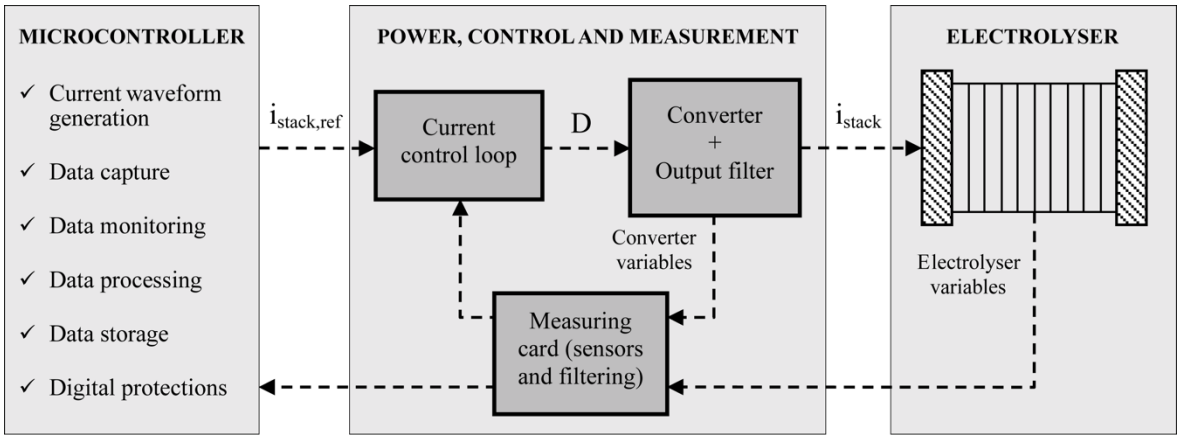

Fig. 3. Overall system description of the EPSE.

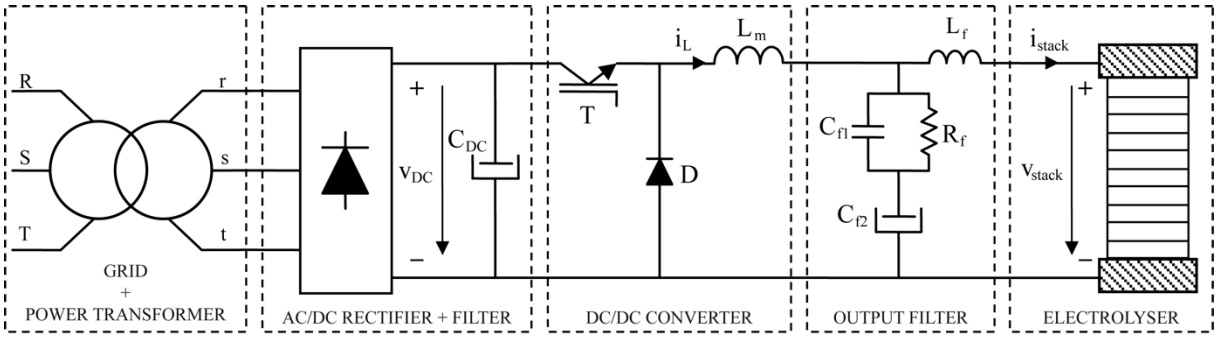

Fig. 4. Scheme of the power stage of the EPSE.

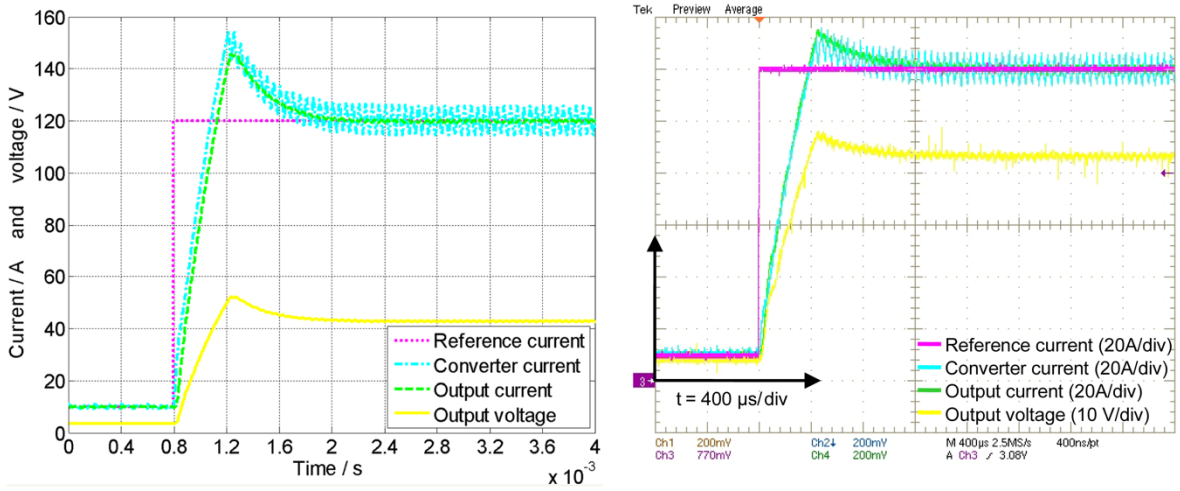

Fig. 5. Simulation (left) and experimental results (right) of the EPSE when faced to a step in the reference current from 10 A to 120 A: reference ($i_{stack,ref}$), converter (i_L) and output (i_{stack}) currents, and output voltage (v_{stack}).

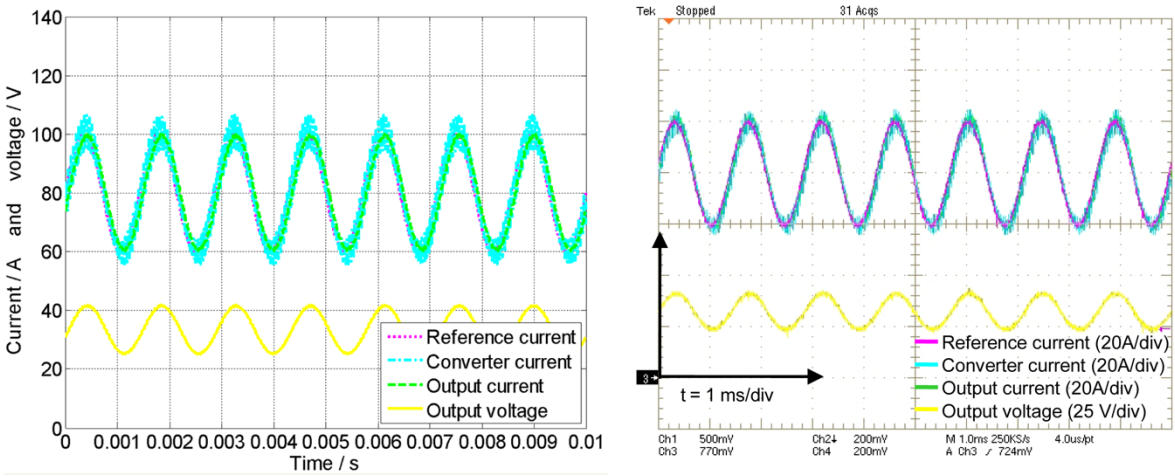

Fig. 6. Simulation (left) and experimental results (right) of the EPSE when the reference current is a 80 A DC-biased sinusoidal waveform of amplitude 20 A and frequency 900 Hz: reference ($i_{stack,ref}$), converter (i_L) and output (i_{stack}) currents, and output voltage (v_{stack}).

Fig. 7. Hydrogenics commercial alkaline water electrolyser H2 IGen 300/1/25.

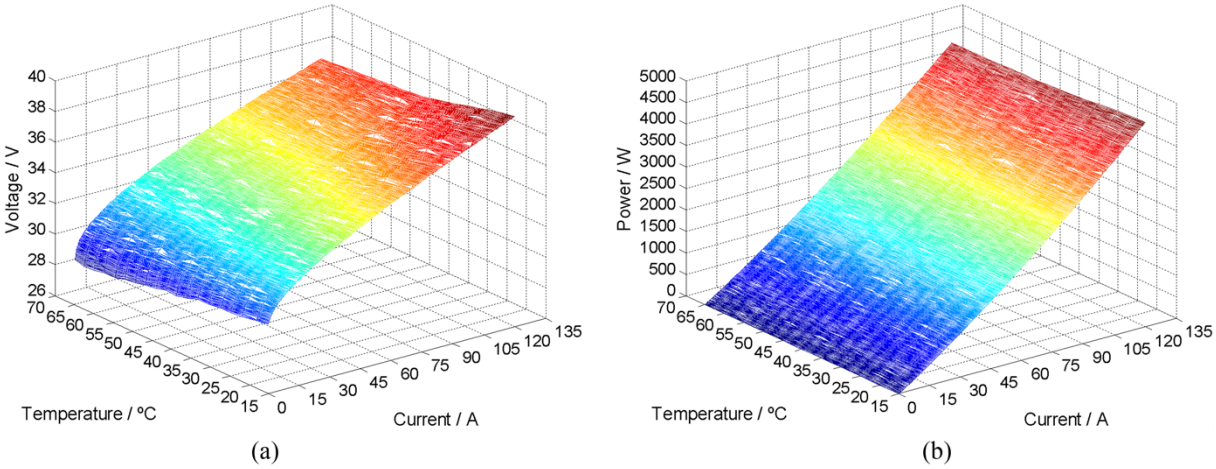

Fig. 8. Experimental electrolyser cell stack *curves* for an absolute operating pressure of 20 bar. (a) Evolution of the *I-V* characteristic curves from 15 to 65 ºC. (b) Evolution of the *I-P* characteristic curves from 15 to 65 ºC.

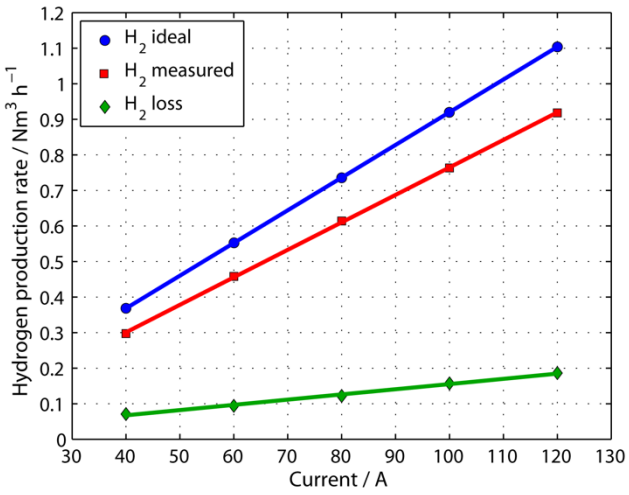

Fig. 9. Electrolyser hydrogen production rate (20 bar and 65 ºC operating conditions).

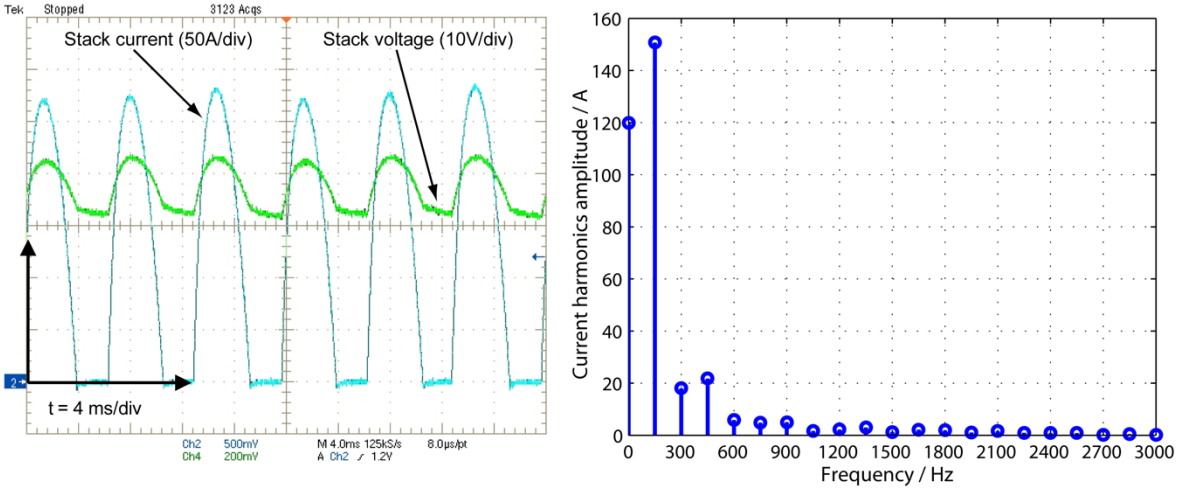

(a) (b)

Fig. 10. Electric supply of a commercial alkaline electrolyser by means of a power supply of the ThPS group. (a) Cell stack current and voltage. (b) Harmonic distribution of the cell stack current.

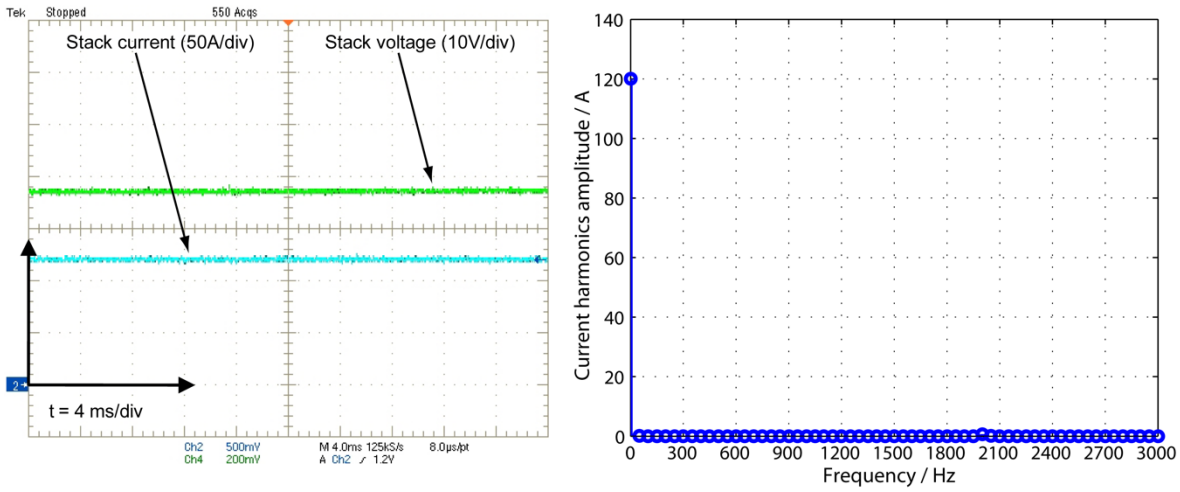

(a) (b)

Fig. 11. Electric supply of a commercial alkaline electrolyser by means of a power supply of the TrPS group. (a) Cell stack current and voltage. (b) Harmonic distribution of the cell stack current.

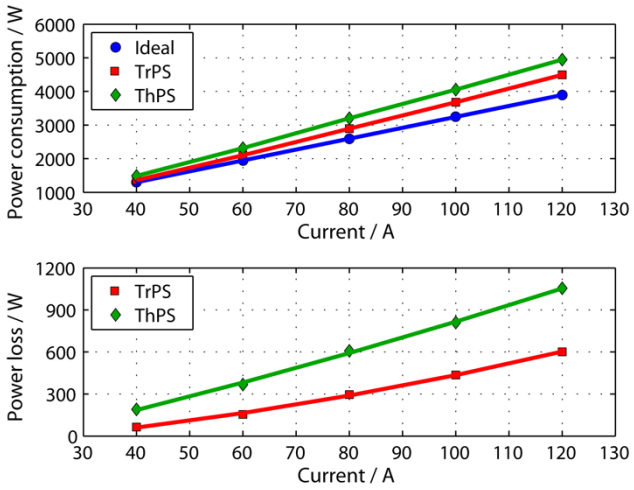

Fig. 12. Electrolyser cell stack power consumption (20 bar and 65 ºC operating conditions).

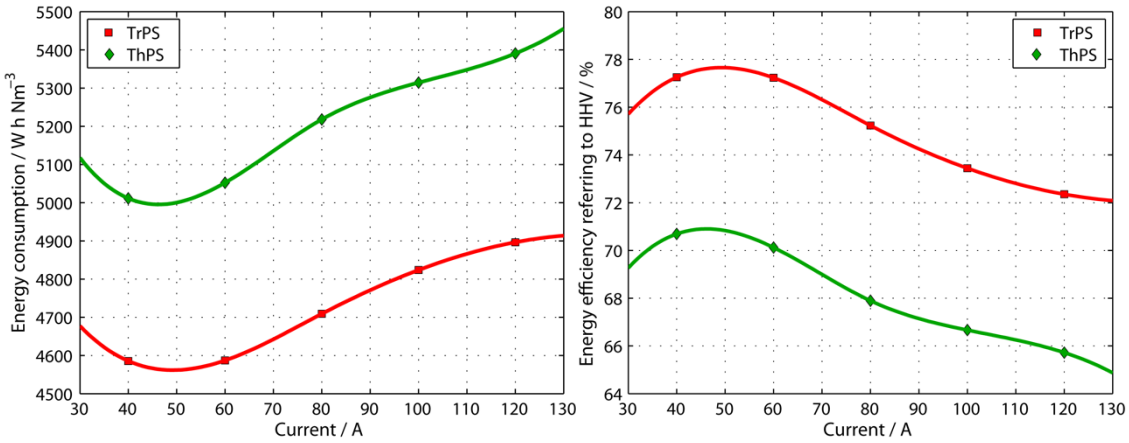

Fig. 13. Electrolyser cell stack energy consumption and efficiency referred to HHV (20 bar and 65 ºC operating conditions).